PLOS COMPUTATIONAL BIOLOGY

RESEARCH ARTICLE

RNA length has a non-trivial effect in the stability of biomolecular condensates formed by RNA-binding proteins

Ignacio Sanchez-Burgos[1☯], **Jorge R. Espinosa**[1☯], **Jerelle A. Joseph**[1,2,3], **Rosana Collepardo-Guevara**[1,2,3*]

1 Maxwell Centre, Cavendish Laboratory, Department of Physics, University of Cambridge, J J Thomson Avenue, Cambridge, United Kingdom, **2** Department of Chemistry, University of Cambridge, Lensfield Road, Cambridge, United Kingdom, **3** Department of Genetics, University of Cambridge, Downing Site, Cambridge, United Kingdom

☯ These authors contributed equally to this work.
* rc597@cam.ac.uk

Citation: Sanchez-Burgos I, Espinosa JR, Joseph JA, Collepardo-Guevara R (2022) RNA length has a non-trivial effect in the stability of biomolecular condensates formed by RNA-binding proteins. PLoS Comput Biol 18(2): e1009810. https://doi.org/10.1371/journal.pcbi.1009810

Editor: Shi-Jie Chen, University of Missouri, UNITED STATES

Received: October 12, 2021

Accepted: January 6, 2022

Published: February 2, 2022

Data Availability Statement: All relevant data are within the manuscript and its Supporting information files. All the codes for our models are already shared in GitHub: https://github.com/CollepardoLab/.

Funding: This project has received funding from the European Research Council (ERC) under the European Union Horizon 2020 research and innovation programme (grant agreement No 803326 to R.C.G). J.R.E. acknowledges funding from the Oppenheimer Fellowship and from

Abstract

Biomolecular condensates formed via liquid–liquid phase separation (LLPS) play a crucial role in the spatiotemporal organization of the cell material. Nucleic acids can act as critical modulators in the stability of these protein condensates. To unveil the role of RNA length in regulating the stability of RNA binding protein (RBP) condensates, we present a multi-scale computational strategy that exploits the advantages of a sequence-dependent coarse-grained representation of proteins and a minimal coarse-grained model wherein proteins are described as patchy colloids. We find that for a constant nucleotide/protein ratio, the protein fused in sarcoma (FUS), which can phase separate on its own—i.e., via homotypic interactions—only exhibits a mild dependency on the RNA strand length. In contrast, the 25-repeat proline-arginine peptide (PR_{25}), which does not undergo LLPS on its own at physiological conditions but instead exhibits complex coacervation with RNA—i.e., via heterotypic interactions—shows a strong dependence on the length of the RNA strands. Our minimal patchy particle simulations suggest that the strikingly different effect of RNA length on homotypic LLPS versus RBP–RNA complex coacervation is general. Phase separation is RNA-length dependent whenever the relative contribution of heterotypic interactions sustaining LLPS is comparable or higher than those stemming from protein homotypic interactions. Taken together, our results contribute to illuminate the intricate physicochemical mechanisms that influence the stability of RBP condensates through RNA inclusion.

Author summary

Liquid–liquid phase separation of proteins and other biomolecules into condensed phases has emerged as a fundamental mechanism to organize biological matter in living cells. Nucleic acids, which are ubiquitously found in condensates, can act as critical

Emmanuel College Roger Ekins Research Fellowship. I.S.B. acknowledges funding from the Oppenheimer Fellowship, EPRSC Doctoral Programme Training number EP/T517847/1 and Derek Brewer Emmanuel College scholarship. J.A. J. is a Junior Research Fellow at Kings College. This work has been performed using resources provided by the Cambridge Tier-2 system operated by the University of Cambridge Research Computing Service (http://www.hpc.cam.ac.uk) funded by EPSRC Tier-2 capital grant EP/P020259/1 (to I.S.B, J.R.E., J.A.J. and R.C.G.). The funders had no role in study design, data collection and analysis, decision to publish, or preparation of the manuscript.

Competing interests: The authors have declared that no competing interests exist.

modulators in the stability of protein condensates. RNA strands can promote or inhibit phase separation of RNA-binding proteins in a concentration-dependent manner. In vivo, RNAs vary enourmously in sequence, structure, and length. Here, we focus on single-stranded disordered RNAs and uncover the role that RNA strand length has in promoting phase separation of RNA-binding proteins. To do so, we develop a multiscale computational strategy that integrates a sequence-dependent protein/RNA coarse-grained model and minimal representation of proteins as patchy particles. Our simulations reveal that phase separation of RNA-binding proteins is RNA-length dependent only when heterotypic protein–RNA interactions have a comparable or higher contribution towards the connectivity of the condensate liquid network than the homotypic protein–protein interactions. Overall, our work sheds light on the molecular and physicochemical mechanisms by which condensate stability is impacted by RNA of different lengths.

Introduction

Cells require precise compartmentalization of their material into different organelles in order to function. While some of these organelles and compartments are shaped by physical membranes, many others are thought to be sustained by liquid–liquid phase separation (LLPS) [1–4]. Like oil and water, biomolecules including multivalent proteins and, in some cases, nucleic acids, can spontaneously demix into phase-separated droplets known as biomolecular condensates [5, 6]. Beyond compartmentalization, numerous vital roles have been recently associated with biomolecular condensates, including cell signaling [2, 7], formation of super-enhancers [8], genome organization [9–12], and aiding cells to sense and react to environmental changes [13], among many others [14–17]. Within the extensive class of biomolecules that can undergo phase separation at physiological conditions, RNA-binding proteins (RBPs), such as FUS [18–20], hnRNPA1 [21, 22], TDP-43 [23–25], TAF-15 [26, 27], G3BP1 [28–31] or EWSR1 [26, 27, 32], have been widely investigated due to their implications in the stability of stress granules [33, 34], P granules [1, 35, 36] and other RNA granules/bodies [37–39].

Phase-separation of RBPs can be both promoted or inhibited by the presence of RNA in an RNA-concentration, and sometimes RNA-structure, dependent manner [27, 32, 40–50]. From the physicochemcial point of view, RBPs possess key features that explain their highly RNA–sensitive phase behaviour. RBPs are multidomain proteins that combine aromatic-rich and arginine-rich intrinsically disordered regions (IDRs) [26, 51]—boosting the RBP's multivalency needed for LLPS—with globular domains that exhibit high affinity for RNA (termed RNA recognition motifs (RRMs)) [52]. Hence, RBPs and RNA can establish both specific RNA- -RRM interactions and non-specific electrostatic, cation–π and π–π interactions. To gain a mechanistic understanding of the intricate modulation of RBP condensate stability by RNA, experiments where single amino acids are mutated and/or post-translationally modified (e.g. phosphorylated [10, 11, 53] or methylated [18, 54, 55]) are of great value. Alongside, sequence-dependent molecular simulations can help uncover how specific protein regions, amino acid-RNA interactions, or RNA properties influence the experimentally observed behavior [49, 50, 56–58].

Computer simulations have been instrumental in advancing the characterization of biomolecular condensates from a thermodynamic, molecular and mechanistic perspective [6, 59–61]. Many approaches, such as atomistic Molecular Dynamics (MD) simulations [61–63],

sequence-dependent coarse-grained models [56, 64–67] or minimal representations of proteins [68–73], as well as lattice-based simulations [74–77] and mean field models [78–82] have been developed and exploited to interrogate biomolecular LLPS. These approaches have shed light on the effects of key parameters in LLPS, encompassing protein length [83, 84], amino acid sequence [56, 64, 65, 85, 86], multivalency [74, 87–93], conformational flexibility [94, 95], and multicomponent composition [49, 69, 96–100]. Moreover, computer simulations have uncovered links between chemical modifications, sequence mutations, and protein–protein or protein–DNA interactions [101–106]. Coarse-grained models have also been employed to investigate the RNA-induced reentrant LLPS behaviour of RBPs [49, 50], the effect of RNA on phase separation of small prion-like domains such as those of FUS, [69, 107], protamine [108] and LAF-1 [49], and the emergence of multiphasic protein–RNA condensates [109].

In this work, we focus on single-stranded disordered RNA and ask: What is the function of RNA strand length in biomolecular LLPS? For this, we use our recently developed residue/nucleotide-resolution coarse-grained protein/RNA model [57], which predicts biomolecular phase diagrams in quantitative agreement with experiments. We demonstrate striking and contrasting effects of RNA length on the phase behaviour of RBPs. For RBPs like FUS, which can undergo LLPS via homotypic protein–protein interactions, low-to-moderate RNA concentrations invariably lead to moderate enhancement of condensate stability, irrespective of the RNA length (for a fixed total nucleotide/protein concentration). In contrast, for RBPs like PR_{25} that undergo RNA-dependent complex coacervation (i.e., LLPS driven by heterotypic protein–RNA interactions), increasing RNA length at constant total nucleotide concentration significantly promotes condensate stability. Next, we use minimal coarse-grained simulations to look at the problem from a soft condensed matter perspective. Our minimal simulations reveal that the striking differences in the impact of RNA length on complex coacervation versus homotypic LLPS originates in the diversity of intermolecular connections that biomolecules employ in the different scenarios to sustain the liquid network of the condensates.

Materials and methods

Multiscale modelling approach for RBP–RNA phase separation

Biomolecular LLPS entails the self-assembly of thousands of different proteins and other biomolecules into liquid-like condensates. Although experiments and simulations have begun to approach condensates at the atomistic level [19,61,110], the study of LLPS is often not amenable to atomistic-level simulations. Instead, coarse-grained models including mean field simulations [78–82, 111], lattice-based models [74–77], and high-resolution sequence-dependent approaches [56, 64–67, 112], are becoming the go-to simulation methods for characterizing the mechanistic and molecular details of biomolecular condensates. Here, we employ two protein/RNA coarse-grained models of different resolutions, previously developed by us, to elucidate the role of RNA length in modulating LLPS of RBPs: (1) the Mpipi sequence-dependent residue-resolution coarse-grained model for proteins and RNA [57], and (2) a minimal model in which proteins are represented as patchy particles, and RNA as self-repulsive flexible polymers [69, 91] (Fig 1).

Within the Mpipi model, protein residues and RNA bases are represented by single beads with unique chemical identities (Fig 1 Left) in which hydrophobic, π–π and cation–π interactions are modelled through a mid-range pairwise potential (Wang–Frenkel potential [113]), and electrostatic interactions via Yukawa long-range potentials [56]. Bonded interactions between sequential amino acids within the same protein, or nucleotides within the same RNA strand, are described with a harmonic potential. Additionally, within Mpipi, the intrinsically

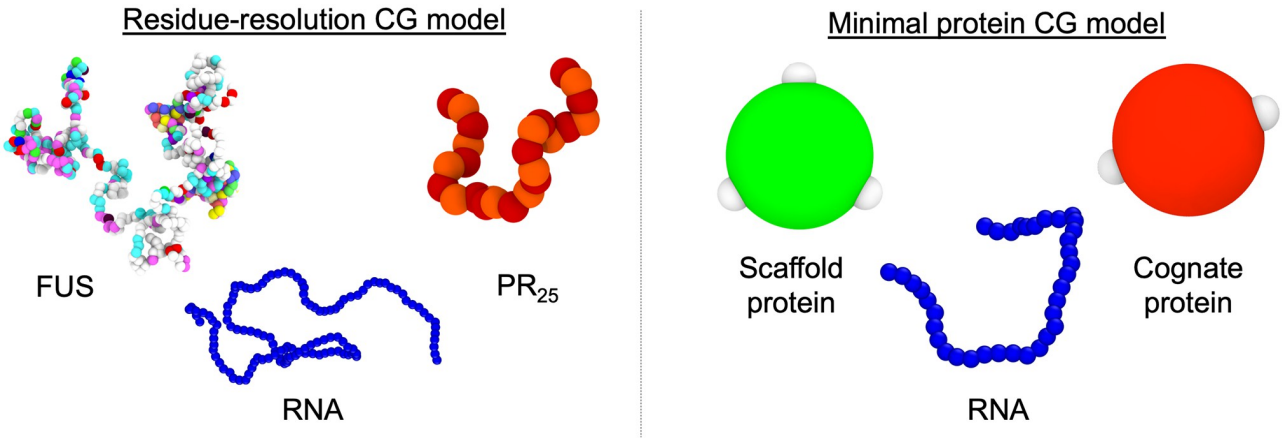

Fig 1. Coarse-grained models used to investigate phase separation of RBP–RNA mixtures. Left: Residue-resolution sequence-dependent coarse-grained representation of full FUS, PR_{25}, and a 400-mer polyU RNA strand, using the Mpipi model [57]. The Mpipi model represents each amino acid and nucleotide by a single bead and describes the solvent implicitly. Please note that the size of the beads represented in this panel have been conviniently rescaled for visualization purposes. Globular protein domains are modelled as rigid bodies based on the crystal structure of the folded domains, whereas disordered protein regions and RNA are treated as fully flexible polymers. Coloured beads indicate distinct types of residues/nucleotides. Right: Minimal model for scaffold proteins, cognate proteins, and RNA, as done previously [69, 91, 120]. White patches represent protein binding sites, while green and red spheres account for the excluded volume of the scaffold and cognate proteins, respectively [91]. RNA is modelled as a self-repulsive flexible polymer of (pseudo) hard-spheres [69]. Please note that the real size of the RNA beads has been intentionally reduced in this image to facilitate its visualization; in the simulations, the size of each RNA bead is the same as the central pseudo hard-sphere of the proteins.

https://doi.org/10.1371/journal.pcbi.1009810.g001

disordered regions of the proteins and RNA strands are treated as fully flexible polymers. Globular domains are described as rigid bodies based on their corresponding experimental atomistic structures taken from the Protein Data Bank (PDB) and adapted to the model resolution. In the Mpipi model, the interactions between 'buried' amino acids within globular domains are scaled down. The physiological concentration of monovalent ions in solution (i.e., $\sim$150 mM NaCl), within the implicit solvent model, is approximated by the screening length of the Yukawa/Debye-Hückel potential. Further details on the model parameters, protein sequences and simulation setups are provided in the S1 Text.

Complementary to the residue-resolution sequence-dependent model, we employ a minimal coarse-grained model [69, 91] to investigate the role of RNA length in RBPs LLPS. Within this model, proteins are described by pseudo hard-sphere (PHS) [115] particles decorated with sticky patches that represent the protein binding sites (modelled through square-well-like potentials [116]); these allow the minimal proteins to establish multivalent transient interactions (Fig 1 Right). Additionally, RNA strands in our minimal model are represented as fully flexible self-repulsive PHS polymers that can interact attractively with RBPs via mid-range non-specific interactions (see S1 Text and Ref. [69] for further details on the model potentials and parameters). Each minimal RNA bead accounts for tens of nucleotides and has the same size as the protein beads [69]. As in the residue-resolution coarse-grained model, an implicit solvent is used; accordingly, the diluted phase (i.e., the protein-poor liquid phase) and the condensed phase (i.e., the protein-rich liquid phase) are effectively a vapor and a liquid phase, respectively.

To measure the stability of the RBP–RNA condensates, we compute phase diagrams of the different systems in the temperature–density plane by means of Direct Coexistence (DC) simulations [117, 118]. Within the DC approach, the two coexisting phases of the system are placed in the same simulation box; in our case, a high-density protein liquid and a very low-density one. We employ a rectangular box, with an elongated side perpendicular to the interfaces (long enough to capture the bulk density of each phase), while the parallel sides are

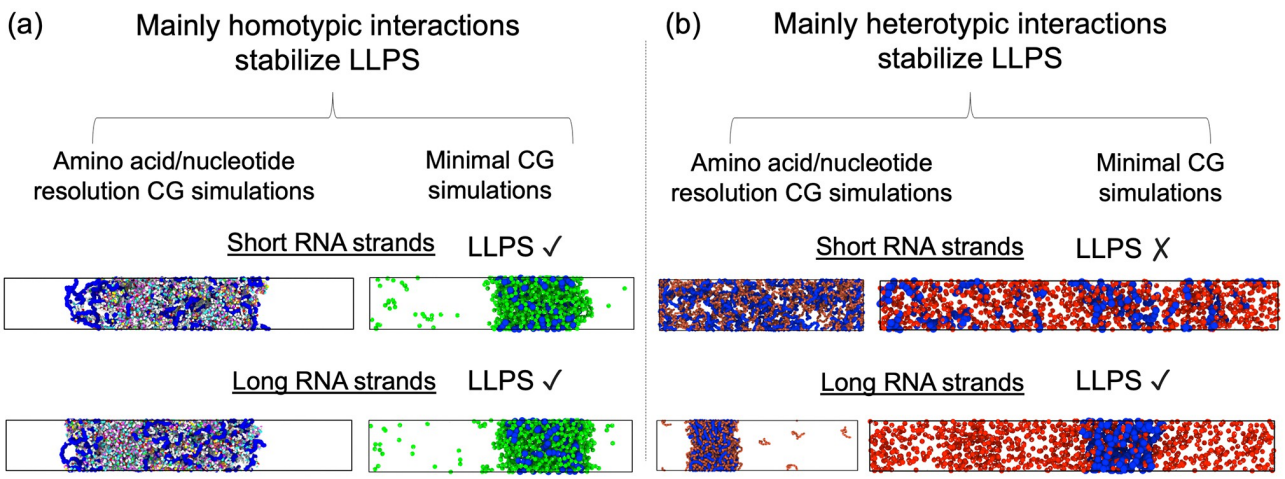

Fig 2. (a) Direct Coexistence simulations of FUS/RNA (left) and scaffold proteins/RNA (right) using short RNA strands (top; 50-mer polyU and 10-bead RNA chains in the FUS and the minimal scaffold protein system respectively) and long RNA strands (bottom; 400-mer and 250-bead RNA chains in the FUS and the minimal scaffold protein system respectively) at $T/T_c = 1.01$, where T_c corresponds to the pure protein critical temperature of each system. (b) Direct Coexistence simulations of PR_{25}/RNA (left) and cognate proteins/RNA (right) using both short RNA strands (top; 40-mer polyU and 10-bead polyU RNA chains in the PR_{25} and RNA cognate protein system respectively) and long RNA strands (bottom; 400-mer and 250-bead RNA chains in the PR_{25} and RNA cognate protein system respectively) at $T/T_c = 1.01$, where T_c corresponds to the pure critical temperature of FUS (left) and scaffold proteins (right), as in panel (a).

https://doi.org/10.1371/journal.pcbi.1009810.g002

chosen such that proteins cannot interact with themselves across the periodic boundaries [50]. We then run *NVT* MD simulations until equilibrium is reached. Once the simulations have converged, we measure the equilibrium coexisting densities of both phases along the long side of the box, excluding the fluctuations of the interfaces and keeping the center of mass of the system fixed. We repeat this procedure at different temperatures until we reach supercritical temperatures, where no phase separation is observed any longer. Then, to avoid finite system-size effects close to the critical point, we evaluate the critical temperature (T_c) and density (ρ_c) using the law of critical exponents and rectilinear diameters [119] (as shown in Refs. [69, 91]). Fig 2(a) (Top and Bottom panels) depicts phase-separated systems computed via DC simulations, while Fig 2(b) (Top panel) shows supercrticial systems (i.e., no phase separation).

Results and discussions

Impact of RNA length in the phase behaviour of FUS *versus* PR_{25} condensates

Using MD simulations of our protein/RNA sequence-specific Mpipi model [57], we first investigate the effect of adding disordered polyU single-stranded RNA chains to RBPs condensates, and varying the length of the polyU (while keeping the total amount of U nucleotides and protein constant). Specifically, we compare the effects of RNA length in the phase behaviour of two different RBPs: (1) FUS, which can phase separate on its own at physiological conditions via homotypic protein–protein interactions, and (2) PR_{25}, which only undergoes LLPS at physiological conditions in the presence of RNA (Fig A in the S1 Text) via heterotypic RNA–protein interactions [48, 103, 114].

For the different FUS/RNA systems, regardless of the length of the RNA strands in each case, we always add a total amount of U nucleotides to get a constant U/FUS mass ratio of 0.096; that is because this ratio enhances phase separation with respect to the pure FUS system. Importantly, the net charge of the system at this RNA/protein mass ratio is very low (−42*e*)

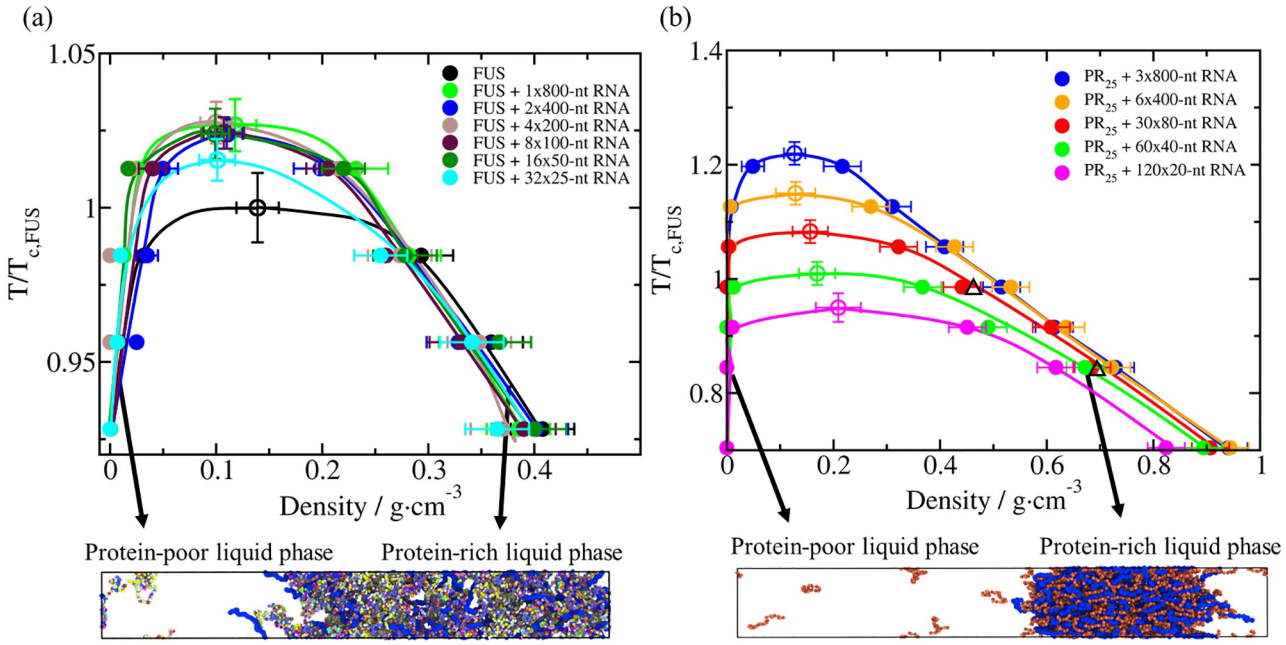

Fig 3. (a) Temperature–density phase diagrams of FUS with polyU RNA of different lengths at a constant polyU/FUS mass ratio of 0.096, and for a pure system of FUS (black curve). The length of polyU RNA strands range from 25-nucleotide to 800-nucleotide. (b) Temperature–density phase diagrams of PR_{25} with RNA at different lengths at a constant RNA/PR_{25} mass ratio of 1.20. RNA lengths range from 20-nucleotide to 800-nucleotide strands. To verify that our simulations are not affected by finite size effects, we repeated our simulations with 60 chains of 80-nt each (instead of 30 polyU chains), while keeping the RNA/PR_{25} mass ratio constant, and computed the coexistence densities (black empty triangles). In both (a) and (b) panels, filled circles represent the coexisting densities evaluated from DC simulations while empty circles depict the critical temperatures estimated from the law of rectilinear diameters and critical exponents [119] near the critical temperature. The error bars in the coexistence densities represent standard deviations, while those of the critical points represent the extrapolated uncertainty when applying the law of rectilinear diameters and critical exponents. Temperature in both panels has been normalized by the critical temperature of pure FUS, $T_{c,FUS}$ = 355 K (black empty circle in (a)). Representative snapshots of the DC simulations used to compute the phase diagrams of both systems for a given RNA strand length (a) FUS–polyU (2x400-nt) and b) PR_{25}–polyU (6x400-nt)) under phase-separating conditions are included below. The same color code employed in Fig 1 applies here.

https://doi.org/10.1371/journal.pcbi.1009810.g003

and has been shown to ensure the maximum condensate stability of FUS as a function of RNA concentration [50]. Specifically, we test six polyU lenghts: (i) 32 polyU chains of 25 nucleotides each, (ii) 16 polyU chains of 50 nucleotides each, (iii) 8 polyU chains of 100 nucleotides each, (iv) 4 polyU chains of 200 nucleotides each, (v) 2 polyU chains of 400 nucleotides each, and (vi) 1 polyU chains of 800 nucleotides each (further details on these systems are provided in Table A of the S1 Text). In all these systems (Fig 3(a)), we observe a moderate increase in the critical temperature of FUS when RNA is added, independently of the length of RNA; i.e., all FUS+polyU systems we simulate have very similar critical temperatures within the uncertainty.

To determine if proteins that phase separate by complex coacervation exhibit a similar trend, we next investigate the effect of RNA length on PR_{25}–polyU mixtures using the Mpipi model. In this case, we fix the polyU/PR_{25} mass ratio to 1.20 (net system charge of 0*e*), which maximizes the size of the coexistence region for the smallest length of polyU used (20 nucleotides). We then test five different polyU lengths: (i) 120 polyU chains of 20 nucleotides each, (ii) 60 polyU chains of 40 nucleotides each, (iii) 30 polyU chains of 80 nucleotides each, (iv) 6 polyU chains of 400 nucleotides each, (v) 3 polyU chains of 800 nucleotides each (further details on these systems are provided in Table A of the S1 Text). The dependence of the phase behaviour of PR_{25} on RNA length is strikingly different (Fig 3(b)): the size of the coexistence region for PR_{25}+polyU now grows continuously as the length of polyU increases. To confirm that our results are not affected by significant finite size effects, we perform additional

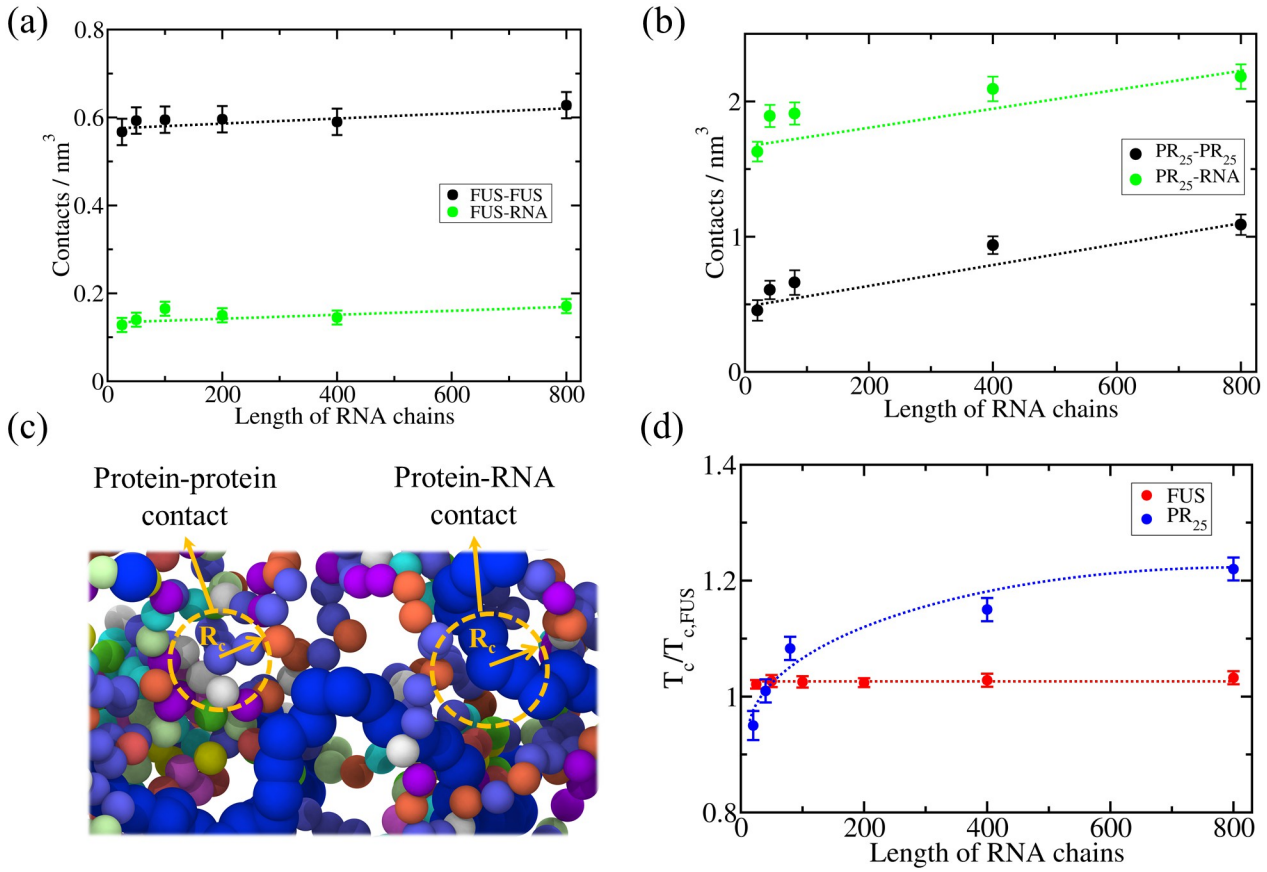

Fig 4. Density of LLPS-stabilizing intermolecular contacts within condensates as a function of RNA length plotted separately for protein–protein interactions (black symbols) and protein–RNA interactions (green symbols) for FUS–polyU (a) and PR_{25}–polyU mixtures (b). The temperature at which the intermolecular contacts were computed was $T/T_{c,FUS} = 0.99$ for FUS–RNA systems, and $T/T_{c,FUS} = 0.85$ for PR_{25}–RNA mixtures. Error bars depict the computed standard deviation in the number of molecular contacts. (c) Representative snapshot of a bulk FUS–polyU condensate to illustrate the employed cut-off distance (R_c) criterion to identify protein- -protein and protein- -RNA contacts. The same color code described in Fig 1 applies here. (d) Critical temperature *versus* RNA length for FUS–RNA (red) and PR_{25}–RNA (blue) systems. The RNA/protein mass ratio of all systems was kept constant at 0.096 for FUS–RNA systems and at 1.20 for PR_{25}–RNA mixtures.

https://doi.org/10.1371/journal.pcbi.1009810.g004

simulations for a system composed of 60 polyU chains of 80 nucleotides each keeping the same polyU/PR_{25} mass ratio (black empty triangles in Fig 3(b)). Indeed, lengthening RNA from 20 to 800 nucleotides increases the critical temperature by as much as 50%. This observation is significant, since while increasing the RNA length, we have maintained a constant nucleotide concentration, which ensures that the total number of binding sites in the RNA molecules available for protein binding is the same in all cases.

To elucidate the molecular origin of this important difference, we compute the percentage of LLPS-stabilizing contacts per unit of volume at 350 K ($T/T_{c,FUS} \sim 1$) for FUS (Fig 4(a)), and 300 K in the case of PR_{25} ($T/T_{c,FUS} \sim 0.85$ (Fig 4(b)). Note that for both systems, we normalize the temperatures using the critical temperature of FUS because PR_{25} cannot phase separate on its own (Fig A in S1 Text). A sketch of the local order parameter to compute the contacts is provided in Fig 4(c). These temperatures were chosen as the highest temperatures at which phase separation is observed for each protein at all RNA lengths. We find that FUS+polyU condensates are mostly stabilized by protein–protein interactions, and more modestly contributed by protein–RNA interactions (Fig 4(a)). Moreover, the contribution of electrostatic interactions to the condensate liquid-network connectivity (including protein–protein and

protein–RNA contacts) is rather modest (< 10%) when compared to non-electrostatic LLPS-stabilizing interactions (Fig G of the S1 Text). Our results suggest that within FUS condensates, where FUS acts as the scaffold, a moderate concentration of RNA creates a few more bridges among the scaffolds; i.e., RNA increases the effective valency of FUS within the condensate or as a co-scaffold in phase separation [121, 122]. In agreement with the well-known RNA concentration-dependent reentrant behaviour of RNA-binding proteins [27, 42, 47, 48], increasing the concentration of polyU in our FUS–polyU simulations, at constant RNA length eventually results in dissolution of the condensates (as shown by simulations in Ref. [50]). At physiological conditions, FUS–FUS interactions are sufficient to drive the system to phase separate [123]. Addition of a moderate amount of RNA creates more connections between FUS proteins by directly binding to free sites on FUS [27] (especially via specific RNA–RRM interactions and promiscous electrostatic and π-π interactions [32, 40–46, 50]. High amounts of RNA begin to outcompete the FUS–FUS connections and introduce electrostatic repulsion, which together eventually inhibit LLPS.

At moderate concentrations, RNA marginally increases the connectivity of an already sufficiently connected condensed liquid network [48]. This is evident from the density of FUS–FUS and FUS–RNA contacts remaining almost constant as the length of the RNA strands increases (Fig 4(a)), following the same trend of critical points as a function of RNA length in the mixtures (Fig 4(d)). We reason that RNA length does not have a strong impact in the stability of FUS condensates because: (1) the total number of FUS–RNA bonds is low enough that the competition between RNA–RNA repulsion among short RNA chains (that would be reduced by the covalent bonds among longer RNA chains) and RNA–FUS attraction becomes unimportant, and (2) FUS is a large protein that offers many distant RNA-binding sites that are equally viable for moderately short RNA chains that repel each other, or for long RNA chains that are stitched together by covalent bonds, as long they have a comparable radius of gyration to that of the proteins [50]. Despite this, we note that experiments have reported how RNA length can modulate the stability of some RNA-binding proteins such as FUS [124] or LAF-1 [125]. However, in those cases the difference in stability was observed at very short lengths (i.e., $\sim$20–40 nucleotides), where the RNA strands were much smaller than the proteins themselves. In fact, when RNA is not long enough to bind to more than one protein at the same time, it can hinder the association with other proteins [50]. Our results argue that for RBPs that exhibit homotypic LLPS (Fig 4(a)), the effect of increasing the RNA length beyond the minimum required to bridge at least two RBPs is expected to be marginal (Fig 4(d)).

In contrast, PR_{25} condensates are mostly stabilized by PR_{25}–polyU interactions (with a higher contribution of electrostatic interactions than those observed in FUS–polyU condensates, Fig G of the S1 Text), and only modestly by protein–protein interactions (Fig 4(b)), as expected from their complex coacervation being dependent on the presence of polyU. We speculate that the considerable abundance of R–U interactions—which significantly facilitate LLPS due to their charge–charge and π–π contributions—might explain the much higher densities of PR_{25}–polyU versus polyU–FUS condensates in our simulations. Indeed, charged-matched in vitro polyR–polyU condensates exhibit very high viscosities [126]. Furthermore, consistent with the increase of the critical temperature with RNA length (Fig 4(d)), the density of protein–RNA intermolecular contacts increases significantly as the RNA lengthens, especially at chain lengths of hundreds of nucleotides (i.e., 800-mer polyU chains in our simulations; Fig 4(b)). Because PR_{25} must bind to RNA to form a liquid network, adding covalent bonds within the RNA chains—for instance, by replacing 40 strands of 20 nucleotides by one strand of 800 nucleotides—increases the PR_{25}+RNA critical temperature by zipping together large chunks of RNA that would otherwise be driven away by the dominant RNA–RNA electrostatic repulsion at physiological conditions. Thus, increasing the length of an RNA chain at

constant nucleotide concentration, allows a higher density of PR_{25} bonds per RNA length, and an overall higher connected condensed liquid.

The distinct behaviour of FUS–polyU *versus* PR_{25}–polyU condensates emerges also with a different residue-resolution coarse-grained model [56] (Figs D and E of the S1 Text). We note also that the behaviour is unlikely explained simply by the RNA strands being longer than PR_{25} peptides in our simulations. Indeed, the FUS–polyU behaviour also holds for long polyU strands of 200-nt with significantly larger radius of gyration for polyU (R_g >100Å) [50] than FUS (Fig C in S1 Text). Furthermore, when approaching the critical temperature of the PR_{25}–polyU mixtures (and also in FUS–polyU mixtures), the number of contacts significantly decreases (Fig F of the S1 Text), independently of the RNA length. A consistent RNA-driven LLPS behaviour, to that observed here, has been experimentally found for the P-granule protein PGL-3, which has limited LLPS propensity in absence of RNA [127]. However, in presence of long (>600-mer) RNA strands, its ability to phase separate increases considerably [127]. Also consistent with our observations, enrichment of long mRNA in stress granules [28, 128, 129] and NEAT1 RNA (∼23000-mer non-coding RNA transcripts) in paraspeckles [130, 131] promotes phase-separation of such membraneless organelles.

RNA length has distinct effects on the stability of condensates driven by homotypic *versus* heterotypic interactions

To test the universality of these observations, we now employ our minimal protein model [69, 98–100], in which proteins are represented as patchy colloids [91] and RNA as a self-repulsive (pseudo hard-sphere) flexible chain [69]. This allows us to go beyond protein sequence and specific molecular features, and assess the thermodynamic parameters that explain the general differences between the impact of RNA length on homotypic phase separation *versus* RNA–protein complex coacervation.

We start by computing the phase diagram of a minimal scaffold protein that, like FUS, is able to phase separate on its own via homotypic interactions. The scaffold protein is represented by a patchy particle decorated with 3-binding sites in a planar arrangement separated by 120 degrees angles (Fig 1 Right). Reducing the behaviour of a multi-domain protein, with its rich conformational ensemble, to a patchy particle is undoubtedly a strong simplification. However, such an approximation allows us to look at the problem from a condensed matter perspective, and identify general parameters that explain the observed behaviour. Indeed, patchy particle models can capture the effects of protein valency, binding affinity, and binding-site topology in the modulation of protein phase diagrams [98, 99, 120]. As shown in Ref. [69], below a reduced temperature of $T^* = 0.09$ (see details on reduced units in S1 Text), the scaffold proteins undergo phase separation (black curve of Fig 5(a)). We note that density is expressed as 'reduced number density', which avoids computing absolute density from the arbitrary choice of the particle mass. To map mass densities from our minimal model to realistic systems, one would need to assign the mass molecule to the patchy particle, and then tune the number of binding-sites, topology, and interaction strength to recapitulate the experimental values. Importantly, we find that with our minimal scaffold model, when adding self-avoiding flexible polymers that mimic RNA, we qualitatively recapitulate the impact on phase behaviour that we observed for FUS (Fig 3(a)) with our residue-resolution coarse-grained simulations. That is, adding a moderate concentration of RNA (a RNA bead/protein ratio of 0.25), increases the critical temperature modestly (by about ∼ 35%), but changing the length of RNA (while keeping the protein/RNA bead concentration constant) has a marginal effect on the critical temperature (Fig 5(a)).

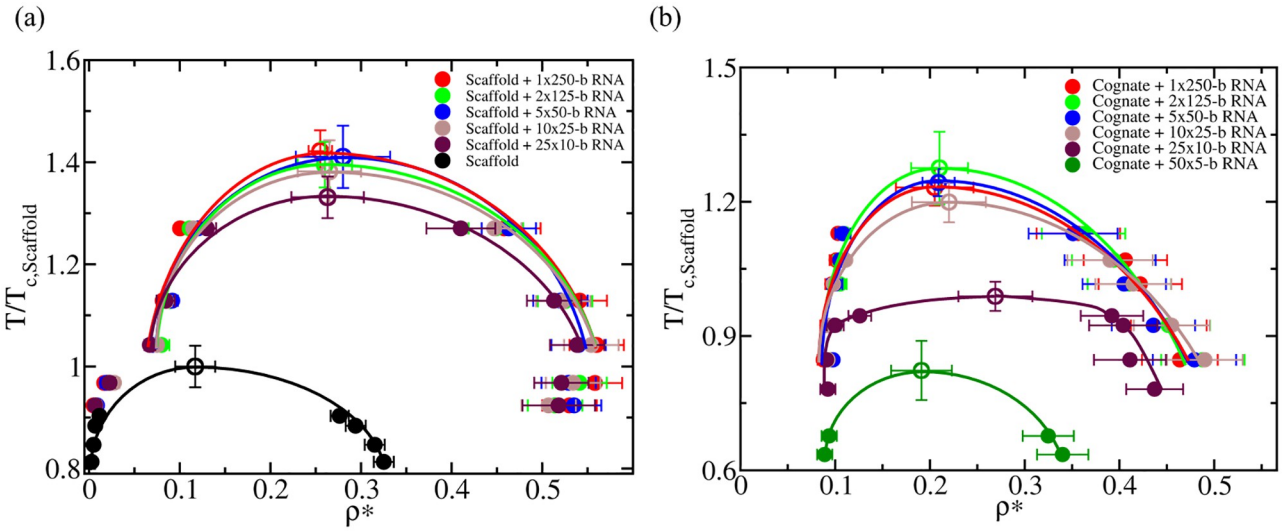

Fig 5. (a) Phase diagram in the temperature–density plane for a scaffold protein that, like FUS, can phase separate via homotypic protein interactions (black curve), and for mixtures of a fixed RNA/protein concentration using different RNA strand lengths as indicated in the legend. (b) Phase diagram in the temperature-density plane for a cognate protein that, like PR_{25}, does not exhibit LLPS on its own, and that only undergoes LLPS upon addition of RNA. The RNA concentration in both panels was kept constant in all simulations at a 0.25 nucleotide/protein ratio. Filled circles represent the coexisting densities evaluated from DC simulations, while empty circles depict the critical temperatures estimated from the law of rectilinear diameters and critical exponents near the critical temperature [119]. The error bars in the coexistence densities represent the standard deviation, while those of the critical points represent the extrapolated uncertainty when applying the law of rectilinear diameters and critical exponents. Temperature in both panels has been normalized by the critical temperature of the pure scaffold system, $T^*_{c,Scaffold} = 0.09$ in reduced units (empty black circle in (a)).

https://doi.org/10.1371/journal.pcbi.1009810.g005

Now we focus on the phase behaviour of a minimal cognate protein that, like PR_{25}, cannot phase separate on its own (Fig 5(b) and Fig B of S1 Text). Our cognate proteins are represented by patchy particles with 2-binding sites in a polar arrangement, which by construction can only form linear chains and not the 3-dimensional percolated network that sustains a condensate [87, 91, 100]). For the minimal cognate proteins, we obtain a phase behavior similar to that of PR_{25}; when increasing the length of RNA (while keeping the RNA bead/protein ratio constant at 0.25), the critical temperature of the mixture considerably increases (Fig 5(b)). However, after reaching a certain RNA length that is much longer that the size of the proteins (i.e., $\sim$50 times longer, which in this minimal model can be tested) [50], the LLPS enhancement plateaus. We have chosen a value of the RNA bead/protein ratio (0.25) that results in RNA-driven enhancement of phase separation. Drastically changing the RNA bead/protein ratio in our minimal simulations can give rise to distinctly different scenarios. On the one hand, very small ratios ($<$0.1), would lead to very minor impact of RNA on condensate stability. On the other, very large ratios (above 0.5 [132]) would result in the coating of RNA with proteins, rather than in the formation of mixed protein–RNA condensates.

Next we analyze the density of protein–protein and protein–RNA contacts as a function of RNA length (Fig 6(a) and 6(b)), to further elucidate the origins of the distinct behavior for scaffold and cognate proteins. We observe a similar trend in terms of the predicted liquid-network connectivity with our minimal model as that found using sequence-dependent coarse-grained simulations (Fig 4(a) and 4(b)), therefore, highlighting the key role of valency in our observations. When LLPS is mainly driven by homotypic scaffold–scaffold interactions, scaffold–scaffold and scaffold–RNA contacts remain roughly constant as the length of RNA increases. In contrast, when LLPS is significantly driven by RNA–protein (i.e., cognate protein) heterotypic interactions, the number of cognate–RNA contacts considerably augments with RNA length (until the RNA size is much larger than that of the proteins; Fig 6(b)). For the

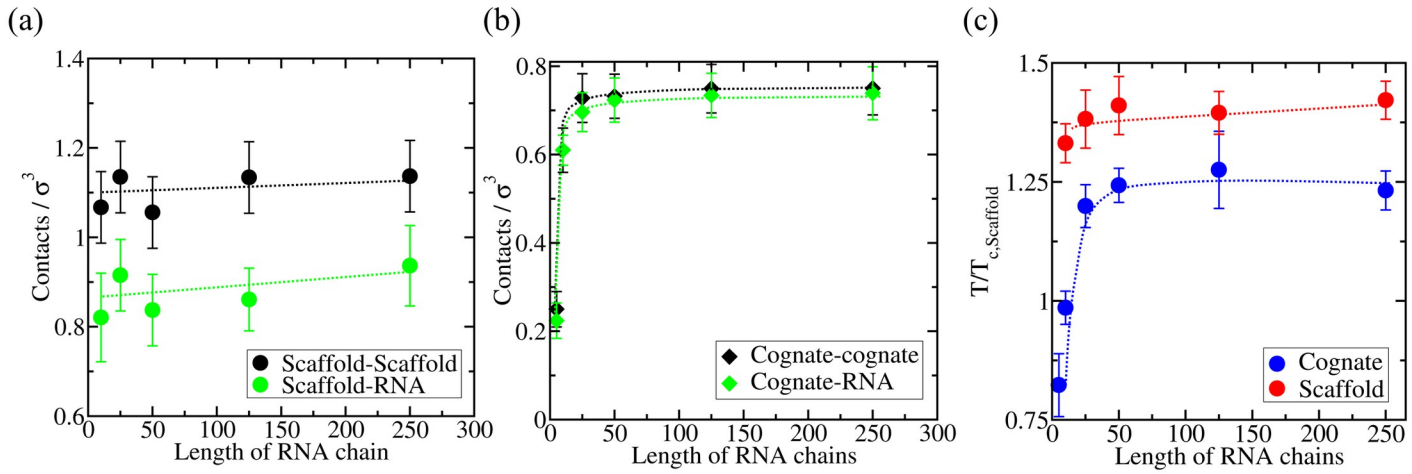

Fig 6. Density of LLPS-stabilizing contacts as a function of RNA length plotted separately for protein–protein contacts (black symbols) and protein–RNA contacts (green symbols) for a minimal RNA-binding scaffold protein model wherein scaffold proteins can phase separate via homotypic interactions (a), and an RNA-binding cognate protein model wherein cognate proteins can only phase separate via heterotypic RNA–protein interactions (b). Calculations are performed at $T/T^*_{c,Scaffold} = 1.13$ for the RNA/scaffold system and $T/T^*_{c,Scaffold} = 0.924$ for the RNA/cognate protein system. Error bars depict the computed standard deviation in the number of molecular contacts. The RNA/protein concentration was kept at a constant nucleotide/protein ratio of 0.25 in both cases. (c) Critical temperature *versus* RNA length plot for both mixtures, scaffold proteins + RNA (red) and cognate proteins + RNA (blue).

https://doi.org/10.1371/journal.pcbi.1009810.g006

minimal scaffold proteins, the increase in scaffold–scaffold and scaffold–RNA contacts with RNA length is smaller than a 5–10% (Fig 6(a)). In contrast, for cognate proteins such increase is higher than a factor of 3, which is a significant difference considering that in both cases RNA/protein ratios are kept constant. The variation in the critical temperature as a function of RNA length is depicted in Fig 6(c), where the consequences of the dissimilar liquid-network connectivity [100] that both type of proteins establish upon demixing—homotypic *vs*. heterotypic interactions—manifest.

In agreement with the preceding results, Zacco *et al.* [25] found that longer RNA strands present weaker dissociation constants with N-RRM1–2 domains of TDP-43 (which, like PR_{25}, cannot phase separate on their own at physiological conditions) than 3-fold shorter RNA strands. Moreover, it has been recently shown that length and charge segregation in the IDR domain of VRN1-like proteins has a critical impact on modulating DNA-induced VRN1 phase separation, where liquid-like, gel-like or no phase-separation behaviour can be favoured depending on the IDR length and the presence of neutral *vs*. charged residues [133]. Another study by Maharana *et al.* [27] showed that smaller RNAs are more potent than larger ones in solubilizing protein condensates at high RNA concentration, which in turn, indirectly supports our observations that very short RNA strands can remotely promote LLPS for proteins that heavily rely on heterotypic interactions. Furthermore, besides controlling condensate stability, RNA has been suggested to play a critical role in regulating the dynamics of many membraneless organelles [21, 27, 32, 134, 135]. In that respect, Zhang *et al.* [136] showed that the RNA-binding protein Whi3 phase separates into liquid-like droplets wherein biophysical properties can be subtly tuned by changing the concentration and length of the mRNA binding partner, finding that larger RNA content increases Whi3 droplet viscosity. RNA has been shown to yield opposite effects in LAF-1 condensates when short strands (50 nt) were introduced [40]. Nonetheless, when long RNAs were used (up to 3,000 nt), LAF-1 condensates presented significantly higher viscosity [41]. Since the impact of RNA length and concentration on condensate density has been recently shown to be a good proxy of condensate dynamics

(i.e., droplet viscosity and protein diffusion) [27, 41, 50], the reported variations in droplet density as a function of RNA length and temperature presented here in Figs 3 and 5, can be also considered as good indicators of the impact that RNA length produces on RBP–RNA droplet transport properties. Therefore, RNA lengths that promote higher droplet density should also lead to enhancements in droplet viscosity [50, 126].

Conclusions

Using a multiscale simulation approach we demonstrate how variations in RNA length can yield non-trivial effects in the stability of RBP condensates. We find that in condensates sustained by homotypic protein–protein interactions, RNA behaves as a LLPS enhancer that subtly augments the stability of the condensates irrespective of its length. In contrast, in condensates sustained by heterotypic protein–RNA interactions, we find that RNA acts as a LLPS enabler that increases the stability of the condensates in a RNA length-dependent manner.

Our findings for FUS and PR_{25} polyU systems using sequence-dependent coarse-grained simulations in parellel with our results for the miminal protein/RNA model suggest that when protein–protein LLPS-stabilising interactions are substantially higher than protein–RNA contacts, like in FUS or in our archetypal scaffold protein model, it is the RNA concentration rather than its chain length what critically modulates the condensate stability (at least for strands larger than 50–80 nucleotides or of comparable length to that of the proteins). Nevertheless, when protein–RNA intermolecular contacts contribute similarly or even higher than homotypic protein–protein interactions, like in PR_{25} peptides or in our minimal cognate–RNA model, not only the RNA concentration, but also the RNA chain length plays a major role in controlling RBP condensate stability. Our study demonstrates that RNA participation in biological phase transitions is not uniform and argues that RNA parameters should be considered as important as those of proteins with respect to the regulation of the stability and mesoscale properties of condensates.

Supporting information

S1 Text. Model description and computational details of the sequence-dependent high-resolution model and the minimal model. Mpipi model, full-FUS sequence, patchy particle protein/RNA model, Direct Coexistence calculations for extracting phase diagrams, and calculation of protein/RNA molecular contacts. **Table A. System sizes and simulation details**. Summary of the simulation details of the employed systems: Total number of proteins (N_P), total number of RNA nucleotides (or RNA beads in the minimal model; N_N), total number of RNA chains ($N_{RNA,chain}$), length of the RNA chains (L_{RNA}), net charge of the system, box dimensions (in x/Å, y/Å, z/Å), and estimated critical temperature (T_c in K for the high-resolution Mpipi model and in reduced units for the minimal CG model). **Fig A. Direct Coexistence simulation of PR_{25} in absence of RNA**. Snapshot of a pure PR_{25} Direct coexistence simulation at $T/T_{c,FUS} = 0.5$. As it can be seen, in absence of RNA, PR_{25} cannot undergo LLPS (even at low temperatures). The same colour code employed in Fig 1 of the main text has been employed here. **Fig B. Direct Coexistence simulation of cognate proteins in absence of RNA**. Snapshot of a pure cognate system Direct Coexistence simulation at $T/T_{c,Scaffold} = 0.6$. As it can be seen, in absence of RNA, the cognate protein cannot undergo LLPS (even at low temperatures). The same colour code employed in Fig 1 of the main text has been employed here. **Fig C. Radius of gyration of FUS and PR_{25}**. Radius of gyration (R_g) distribution function for: a) FUS within a FUS-polyU(400-nt) condensate (green curve) and FUS in the dilute phase (black curve) at $T/T_{c,FUS} = 0.96$. b) PR_{25} within a PR_{25}-polyU(400-nt) condensate (green curve) and PR_{25} in the dilute phase (black curve) at $T/T_{c,FUS} = 0.85$. The polyU/FUS mass ratio

was kept constant at a value of 0.096, while the polyU/PR_{25} mass ratio at a value of 1.20. **Fig D. Phase diagrams of FUS-polyU and PR_{25}-polyU mixtures using the HPS and KH models**. Temperature–density phase diagrams of FUS with polyU of different lengths at a constant polyU/FUS mass ratio of 0.16, and for a pure system of FUS (black curve). (b) Temperature–density phase diagrams of PR_{25} with RNA at different lengths at a constant RNA/PR_{25} mass ratio of 0.57. In both (a) and (b) panels, filled circles represent the coexisting densities evaluated from DC simulations while empty circles depict the critical temperatures estimated from the law of rectilinear diameters and critical exponents near the critical temperature. Temperature in both panels has been normalized by the critical temperature of pure FUS, $T_{c,FUS}$ = 309K (black empty circle in (a)). **Fig E. Intermolecular contacts of FUS-polyU and PR_{25}-polyU condensates using the HPS and KH models**. Density of LLPS-stabilizing intermolecular contacts within condensates as a function of RNA length plotted separately for protein–protein interactions (black symbols) and protein–RNA interactions (green symbols) for FUS-polyU (a) and PR_{25}-polyU mixtures (b). The temperature at which the intermolecular contacts were computed was $T/T_{c,FUS}$ = 1.13 for FUS–RNA systems and $T/T_{c,FUS}$ = 0.924 for PR_{25}–RNA mixtures (the highest temperature at which all systems with distinct RNA lengths can phase separate). (c) Critical temperature *versus* RNA length for FUS–RNA (black) and PR_{25}–RNA (blue) systems. **Fig F. Intermolecular contacts of FUS-polyU and PR_{25}-polyU condensates as a function of temperature (Mpipi model)**. Density of LLPS-stabilizing intermolecular contacts within the condensates (plotted separately for protein–protein interactions, black circles, and protein–RNA interactions, red circles) as a function of temperature ($T/T_{c,FUS}$) for: a) FUS +polyU(400-nt), and b) PR_{25}+polyU(400-nt) condensates. The polyU/FUS mass ratio was kept constant at a value of 0.096 for all FUS simulations, while the polyU/PR_{25} mass ratio was kept constant at a value of 1.20 for all PR_{25} simulations at every studied temperature. **Fig G. Electrostatic *vs*. non-electrostatic interactions in FUS-polyU and PR_{25}-polyU condensates**. Electrostatic (black symbols) *vs*. non-electrostatic (red symbols) contribution to the potential attractive interactions (molecular contacts sustaining phase-separated condensates) as a function of RNA length for FUS+polyU condensates (filled circles) and PR_{25}+polyU condensates (empty squares). The temperature at which the intermolecular contacts were computed was $T/T_{c,FUS}$ = 0.99 for FUS–RNA systems, and $T/T_{c,FUS}$ = 0.85 for PR_{25}–RNA mixtures. Error bars depict the computed standard deviation in the percentage contribution of electrostatic *vs*. non-electrostatic interactions. The polyU/FUS mass ratio was kept constant at a value of 0.096 for FUS-polyU simulations, and at a polyU/PR_{25} mass ratio of 1.20 in PR_{25}-polyU simulations. (PDF)

Author Contributions

Conceptualization: Jorge R. Espinosa, Rosana Collepardo-Guevara.

Formal analysis: Ignacio Sanchez-Burgos, Jorge R. Espinosa.

Funding acquisition: Jorge R. Espinosa, Rosana Collepardo-Guevara.

Investigation: Ignacio Sanchez-Burgos, Jorge R. Espinosa, Jerelle A. Joseph.

Methodology: Ignacio Sanchez-Burgos, Jorge R. Espinosa, Jerelle A. Joseph.

Project administration: Rosana Collepardo-Guevara.

Software: Ignacio Sanchez-Burgos, Jorge R. Espinosa, Jerelle A. Joseph.

Supervision: Jorge R. Espinosa, Rosana Collepardo-Guevara.

Writing – original draft: Ignacio Sanchez-Burgos, Jorge R. Espinosa, Rosana Collepardo-Guevara.

Writing – review & editing: Ignacio Sanchez-Burgos, Jorge R. Espinosa, Jerelle A. Joseph, Rosana Collepardo-Guevara.

References

1. Brangwynne CP, Eckmann CR, Courson DS, Rybarska A, Hoege C, Gharakhani J, et al. Germline P Granules Are Liquid Droplets That Localize by Controlled Dissolution/Condensation. 2009; 324 (5935):1729–1732.
2. Li P, Banjade S, Cheng HC, Kim S, Chen B, Guo L, et al. Phase transitions in the assembly of multivalent signalling proteins. Nature. 2012; 483(7389):336–340. https://doi.org/10.1038/nature10879 PMID: 22398450
3. Hyman AA, Weber CA, Jülicher F. Liquid-liquid phase separation in biology. Annual review of cell and developmental biology. 2014; 30:39–58. https://doi.org/10.1146/annurev-cellbio-100913-013325 PMID: 25288112
4. Banani SF, Lee HO, Hyman AA, Rosen MK. Biomolecular condensates: organizers of cellular biochemistry. Nature reviews Molecular cell biology. 2017; 18(5):285–298. https://doi.org/10.1038/nrm.2017.7 PMID: 28225081
5. Shin Y, Brangwynne CP. Liquid phase condensation in cell physiology and disease. Science. 2017; 357 (6357). https://doi.org/10.1126/science.aaf4382 PMID: 28935776
6. Alberti S, Gladfelter A, Mittag T. Considerations and challenges in studying liquid-liquid phase separation and biomolecular condensates. Cell. 2019; 176(3):419–434. https://doi.org/10.1016/j.cell.2018.12.035 PMID: 30682370
7. Su X, Ditlev JA, Hui E, Xing W, Banjade S, Okrut J, et al. Phase separation of signaling molecules promotes T cell receptor signal transduction. Science. 2016; 352(6285):595–599. https://doi.org/10.1126/science.aad9964 PMID: 27056844
8. Sabari BR, Dall'Agnese A, Boija A, Klein IA, Coffey EL, Shrinivas K, et al. Coactivator condensation at super-enhancers links phase separation and gene control. Science. 2018; 361 (6400). https://doi.org/10.1126/science.aar3958 PMID: 29930091
9. Larson AG, Narlikar GJ. The Role of Phase Separation in Heterochromatin Formation, Function, and Regulation; 2018.
10. Larson AG, Elnatan D, Keenen MM, Trnka MJ, Johnston JB, Burlingame AL, et al. Liquid droplet formation by HP1α suggests a role for phase separation in heterochromatin. Nature. 2017; 547 (7662):236–240. https://doi.org/10.1038/nature22822 PMID: 28636604
11. Strom AR, Emelyanov AV, Mir M, Fyodorov DV, Darzacq X, Karpen GH. Phase separation drives heterochromatin domain formation. Nature. 2017; 547(7662):241–245. https://doi.org/10.1038/nature22989 PMID: 28636597
12. Sanulli S, Trnka M, Dharmarajan V, Tibble R, Pascal B, Burlingame A, et al. HP1 reshapes nucleosome core to promote phase separation of heterochromatin. Nature. 2019; 575(7782):390–394. https://doi.org/10.1038/s41586-019-1669-2 PMID: 31618757
13. Yoo H, Triandafillou C, Drummond DA. Cellular sensing by phase separation: Using the process, not just the products. Journal of Biological Chemistry. 2019; 294(18):7151–7159. https://doi.org/10.1074/jbc.TM118.001191
14. Sheu-Gruttadauria J, MacRae IJ. Phase transitions in the assembly and function of human miRISC. Cell. 2018; 173(4):946–957. https://doi.org/10.1016/j.cell.2018.02.051 PMID: 29576456
15. Franzmann TM, Alberti S. Prion-like low-complexity sequences: Key regulators of protein solubility and phase behavior. Journal of Biological Chemistry. 2019; 294(18):7128–7136. https://doi.org/10.1074/jbc.TM118.001190 PMID: 29921587
16. Kroschwald S, Munder MC, Maharana S, Franzmann TM, Richter D, Ruer M, et al. Different material states of Pub1 condensates define distinct modes of stress adaptation and recovery. Cell reports. 2018; 23(11):3327–3339. https://doi.org/10.1016/j.celrep.2018.05.041 PMID: 29898402
17. Bouchard JJ, Otero JH, Scott DC, Szulc E, Martin EW, Sabri N, et al. Cancer mutations of the tumor suppressor SPOP disrupt the formation of active, phase-separated compartments. Molecular cell. 2018; 72(1):19–36. https://doi.org/10.1016/j.molcel.2018.08.027 PMID: 30244836
18. Qamar S, Wang G, Randle SJ, Ruggeri FS, Varela JA, Lin JQ, et al. FUS phase separation is modulated by a molecular chaperone and methylation of arginine cation-π interactions. Cell. 2018; 173 (3):720–734. https://doi.org/10.1016/j.cell.2018.03.056 PMID: 29677515

19. Murthy AC, Dignon GL, Kan Y, Zerze GH, Parekh SH, Mittal J, et al. Molecular interactions underlying liquid- liquid phase separation of the FUS low-complexity domain. Nature structural & molecular biology. 2019; 26(7):637–648. https://doi.org/10.1038/s41594-019-0250-x PMID: 31270472

20. Rhoads SN, Monahan ZT, Yee DS, Shewmaker FP. The role of post-translational modifications on prion-like aggregation and liquid-phase separation of FUS. International journal of molecular sciences. 2018; 19(3):886. https://doi.org/10.3390/ijms19030886 PMID: 29547565

21. Molliex A, Temirov J, Lee J, Coughlin M, Kanagaraj AP, Kim HJ, et al. Phase separation by low complexity domains promotes stress granule assembly and drives pathological fibrillization. Cell. 2015; 163(1):123–133. https://doi.org/10.1016/j.cell.2015.09.015 PMID: 26406374

22. Gui X, Luo F, Li Y, Zhou H, Qin Z, Liu Z, et al. Structural basis for reversible amyloids of hnRNPA1 elucidates their role in stress granule assembly. Nature communications. 2019; 10(1):1–12. https://doi.org/10.1038/s41467-019-09902-7 PMID: 31043593

23. Li HR, Chiang WC, Chou PC, Wang WJ, Huang Jr. TAR DNA-binding protein 43 (TDP-43) liquid–liquid phase separation is mediated by just a few aromatic residues. Journal of Biological Chemistry. 2018; 293(16):6090–6098. https://doi.org/10.1074/jbc.AC117.001037 PMID: 29511089

24. McGurk L, Gomes E, Guo L, Mojsilovic-Petrovic J, Tran V, Kalb RG, et al. Poly (ADP-ribose) prevents pathological phase separation of TDP-43 by promoting liquid demixing and stress granule localization. Molecular cell. 2018; 71(5):703–717. https://doi.org/10.1016/j.molcel.2018.07.002 PMID: 30100264

25. Zacco E, Graña-Montes R, Martin SR, de Groot NS, Alfano C, Tartaglia GG, et al. RNA as a key factor in driving or preventing self-assembly of the TAR DNA-binding protein 43. Journal of molecular biology. 2019; 431(8):1671–1688. https://doi.org/10.1016/j.jmb.2019.01.028 PMID: 30742796

26. Wang J, Choi JM, Holehouse AS, Lee HO, Zhang X, Jahnel M, et al. A molecular grammar governing the driving forces for phase separation of prion-like RNA binding proteins. Cell. 2018; 174(3):688–699. https://doi.org/10.1016/j.cell.2018.06.006 PMID: 29961577

27. Maharana S, Wang J, Papadopoulos DK, Richter D, Pozniakovsky A, Poser I, et al. RNA buffers the phase separation behavior of prion-like RNA binding proteins. Science. 2018; 360(6391):918–921. https://doi.org/10.1126/science.aar7366 PMID: 29650702

28. Yang P, Mathieu C, Kolaitis RM, Zhang P, Messing J, Yurtsever U, et al. G3BP1 is a tunable switch that triggers phase separation to assemble stress granules. Cell. 2020; 181(2):325–345. https://doi.org/10.1016/j.cell.2020.03.046 PMID: 32302571

29. Gwon Y, Maxwell BA, Kolaitis RM, Zhang P, Kim HJ, Taylor JP. Ubiquitination of G3BP1 mediates stress granule disassembly in a context-specific manner. Science. 2021; 372 (6549). https://doi.org/10.1126/science.abf6548

30. Sanders DW, Kedersha N, Lee DS, Strom AR, Drake V, Riback JA, et al. Competing protein-RNA interaction networks control multiphase intracellular organization. Cell. 2020; 181(2):306–324. https://doi.org/10.1016/j.cell.2020.03.050 PMID: 32302570

31. Guillén-Boixet J, Kopach A, Holehouse AS, Wittmann S, Jahnel M, Schlüßler R, et al. RNA-induced conformational switching and clustering of G3BP drive stress granule assembly by condensation. Cell. 2020; 181(2):346–361. https://doi.org/10.1016/j.cell.2020.03.049 PMID: 32302572

32. Guo L, Shorter J. It's raining liquids: RNA tunes viscoelasticity and dynamics of membraneless organelles. Molecular cell. 2015; 60(2):189–192. https://doi.org/10.1016/j.molcel.2015.10.006 PMID: 26474062

33. Protter DS, Parker R. Principles and properties of stress granules. Trends in cell biology. 2016; 26 (9):668–679. https://doi.org/10.1016/j.tcb.2016.05.004 PMID: 27289443

34. Li YR, King OD, Shorter J, Gitler AD. Stress granules as crucibles of ALS pathogenesis. Journal of cell biology. 2013; 201(3):361–372. https://doi.org/10.1083/jcb.201302044 PMID: 23629963

35. Schisa JA, Pitt JN, Priess JR. Analysis of RNA associated with P granules in germ cells of C. elegans adults. Development. 2001; 128(8):1287–1298. https://doi.org/10.1242/dev.128.8.1287 PMID: 11262230

36. Folkmann AW, Putnam A, Lee CF, Seydoux G. Regulation of biomolecular condensates by interfacial protein clusters. Science. 2021; 373(6560):1218–1224. https://doi.org/10.1126/science.abg7071 PMID: 34516789

37. Moser JJ, Fritzler MJ. Cytoplasmic ribonucleoprotein (RNP) bodies and their relationship to GW/P bodies. The international journal of biochemistry & cell biology. 2010; 42(6):828–843. https://doi.org/10.1016/j.biocel.2009.11.018 PMID: 19944184

38. Feric M, Brangwynne CP. A nuclear F-actin scaffold stabilizes ribonucleoprotein droplets against gravity in large cells. Nature cell biology. 2013; 15(10):1253–1259. https://doi.org/10.1038/ncb2830 PMID: 23995731

39. Kato M, Han TW, Xie S, Shi K, Du X, Wu LC, et al. Cell-free formation of RNA granules: low complexity sequence domains form dynamic fibers within hydrogels. Cell. 2012; 149(4):753–767. https://doi.org/10.1016/j.cell.2012.04.017 PMID: 22579281

40. Elbaum-Garfinkle S, Kim Y, Szczepaniak K, Chen CCH, Eckmann CR, Myong S, et al. The disordered P granule protein LAF-1 drives phase separation into droplets with tunable viscosity and dynamics. Proceedings of the National Academy of Sciences. 2015; 112(23):7189–7194. https://doi.org/10.1073/pnas.1504822112 PMID: 26015579

41. Wei MT, Elbaum-Garfinkle S, Holehouse AS, Chen CCH, Feric M, Arnold CB, et al. Phase behaviour of disordered proteins underlying low density and high permeability of liquid organelles. Nature Chemistry. 2017; 9(11):1118. https://doi.org/10.1038/nchem.2803 PMID: 29064502

42. Burke KA, Janke AM, Rhine CL, Fawzi NL. Residue-by-residue view of in vitro FUS granules that bind the C-terminal domain of RNA polymerase II. Molecular cell. 2015; 60(2):231–241. https://doi.org/10.1016/j.molcel.2015.09.006 PMID: 26455390

43. Alshareedah I, Kaur T, Ngo J, Seppala H, Kounatse LAD, Wang W, et al. Interplay between Short-Range Attraction and Long-Range Repulsion Controls Reentrant Liquid Condensation of Ribonucleoprotein–RNA Complexes. Journal of the American Chemical Society. 2019; 141(37):14593–14602. https://doi.org/10.1021/jacs.9b03689 PMID: 31437398

44. Matsui S, Nozawa RS. RNA impacts formation of biomolecular condensates in the nucleus. Biomedical Research. 2021; 42(4):153–160. https://doi.org/10.2220/biomedres.42.153 PMID: 34380923

45. Kuechler ER, Budzyńska PM, Bernardini JP, Gsponer J, Mayor T. Distinct features of stress granule proteins predict localization in membraneless organelles. Journal of molecular biology. 2020; 432(7):2349–2368. https://doi.org/10.1016/j.jmb.2020.02.020 PMID: 32105731

46. Chong PA, Vernon RM, Forman-Kay JD. RGG/RG motif regions in RNA binding and phase separation. Journal of molecular biology. 2018; 430(23):4650–4665. https://doi.org/10.1016/j.jmb.2018.06.014 PMID: 29913160

47. Schwartz JC, Wang X, Podell ER, Cech TR. RNA seeds higher-order assembly of FUS protein. Cell reports. 2013; 5(4):918–925. https://doi.org/10.1016/j.celrep.2013.11.017 PMID: 24268778

48. Banerjee PR, Milin AN, Moosa MM, Onuchic PL, Deniz AA. Reentrant phase transition drives dynamic substructure formation in ribonucleoprotein droplets. Angewandte Chemie. 2017; 129(38):11512–11517. https://doi.org/10.1002/anie.201703191 PMID: 28556382

49. Regy RM, Dignon GL, Zheng W, Kim YC, Mittal J. Sequence dependent phase separation of protein-polynucleotide mixtures elucidated using molecular simulations. Nucleic Acids Research. 2020; 48(22):12593–12603. https://doi.org/10.1093/nar/gkaa1099 PMID: 33264400

50. Tejedor AR, Garaizar A, Ramírez J, Espinosa JR. RNA modulation of transport properties and stability in phase separated condensates. Biophysical Journal. 2021;. https://doi.org/10.1016/j.bpj.2021.11.003 PMID: 34762868

51. Bremer A, Farag M, Borcherds WM, Peran I, Martin EW, Pappu RV, et al. Deciphering how naturally occurring sequence features impact the phase behaviors of disordered prion-like domains. bioRxiv. 2021;. PMID: 34931046

52. Cléry A, Blatter M, Allain FH. RNA recognition motifs: boring? Not quite. Current opinion in structural biology. 2008; 18(3):290–298. https://doi.org/10.1016/j.sbi.2008.04.002 PMID: 18515081

53. Monahan Z, Ryan VH, Janke AM, Burke KA, Rhoads SN, Zerze GH, et al. Phosphorylation of the FUS low-complexity domain disrupts phase separation, aggregation, and toxicity. The EMBO journal. 2017; 36(20):2951–2967. https://doi.org/10.15252/embj.201696394 PMID: 28790177

54. Hofweber M, Hutten S, Bourgeois B, Spreitzer E, Niedner-Boblenz A, Schifferer M, et al. Phase separation of FUS is suppressed by its nuclear import receptor and arginine methylation. Cell. 2018; 173(3):706–719. https://doi.org/10.1016/j.cell.2018.03.004 PMID: 29677514

55. Ryan VH, Dignon GL, Zerze GH, Chabata CV, Silva R, Conicella AE, et al. Mechanistic view of hnRNPA2 low-complexity domain structure, interactions, and phase separation altered by mutation and arginine methylation. Molecular cell. 2018; 69(3):465–479. https://doi.org/10.1016/j.molcel.2017.12.022 PMID: 29358076

56. Dignon GL, Zheng W, Best RB, Kim YC, Mittal J. Relation between single-molecule properties and phase behavior of intrinsically disordered proteins. Proceedings of the National Academy of Sciences. 2018; 115(40):9929–9934. https://doi.org/10.1073/pnas.1804177115 PMID: 30217894

57. Joseph JA, Reinhardt A, Aguirre A, Chew PY, Russell KO, Espinosa JR, et al. Physics-driven coarse-grained model for biomolecular phase separation with near-quantitative accuracy. Nature Computational Science. 2021; 1:732–743. https://doi.org/10.1038/s43588-021-00155-3

58. Das S, Lin YH, Vernon RM, Forman-Kay JD, Chan HS. Comparative Roles of Charge, π, and Hydrophobic Interactions in Sequence-Dependent Phase Separation of Intrinsically Disordered Proteins. arXiv preprint arXiv:200506712. 2020.

59. Dignon GL, Best RB, Mittal J. Biomolecular Phase Separation: From Molecular Driving Forces to Macroscopic Properties. Annual Review of Physical Chemistry. 2020; 71:53–75. https://doi.org/10.1146/annurev-physchem-071819-113553 PMID: 32312191

60. Roberts S, Miao V, Costa S, Simon J, Kelly G, Shah T, et al. Complex microparticle architectures from stimuli-responsive intrinsically disordered proteins. Nature communications. 2020; 11. https://doi.org/10.1038/s41467-020-15128-9 PMID: 32165622

61. Paloni M, Bailly R, Ciandrini L, Barducci A. Unraveling Molecular Interactions in Liquid–Liquid Phase Separation of Disordered Proteins by Atomistic Simulations. The Journal of Physical Chemistry B. 2020; 124(41):9009–9016. https://doi.org/10.1021/acs.jpcb.0c06288 PMID: 32936641

62. Shaw DE, Maragakis P, Lindorff-Larsen K, Piana S, Dror RO, Eastwood MP, et al. The Science of Crystallization: Microscopic Phenomena and Defect Generation. Proc Natl Acad Sci USA. 2006; 82 (11):36.

63. Lindorff-Larsen K, Piana S, Dror RO, Shaw DE. How Fast-Folding Proteins Fold. Science. 2011; 334 (6055):517–520. https://doi.org/10.1126/science.1208351 PMID: 22034434

64. Statt A, Casademunt H, Brangwynne CP, Panagiotopoulos AZ. Model for disordered proteins with strongly sequence-dependent liquid phase behavior. The Journal of Chemical Physics. 2020; 152 (7):075101. https://doi.org/10.1063/1.5141095 PMID: 32087632

65. Dignon GL, Zheng W, Kim YC, Best RB, Mittal J. Sequence determinants of protein phase behavior from a coarse-grained model. PLoS computational biology. 2018; 14(1):e1005941. https://doi.org/10.1371/journal.pcbi.1005941 PMID: 29364893

66. Perdikari TM, Jovic N, Dignon GL, Kim YC, Fawzi NL, Mittal J. A predictive coarse-grained model for position-specific effects of post-translational modifications. Biophysical Journal. 2021. https://doi.org/10.1016/j.bpj.2021.01.034 PMID: 33582133

67. Regy RM, Thompson J, Kim YC, Mittal J. Improved coarse-grained model for studying sequence dependent phase separation of disordered proteins. Protein Science. 2021;. https://doi.org/10.1002/pro.4094 PMID: 33934416

68. Liu H, Kumar SK, Sciortino F. Vapor-liquid coexistence of patchy models: relevance to protein phase behavior. The Journal of chemical physics. 2007; 127(8):084902. https://doi.org/10.1063/1.2768056 PMID: 17764289

69. Joseph JA, Espinosa JR, Sanchez-Burgos I, Garaizar A, Frenkel D, Collepardo-Guevara R. Thermodynamics and kinetics of phase separation of protein–RNA mixtures by a minimal model. Biophysical Journal. 2021; 120:1–12. https://doi.org/10.1016/j.bpj.2021.01.031 PMID: 33571491

70. Russo J, Tartaglia P, Sciortino F. Reversible gels of patchy particles: role of the valence. The Journal of chemical physics. 2009; 131(1):014504. https://doi.org/10.1063/1.3153843 PMID: 19586107

71. Nguemaha V, Zhou HX. Liquid-liquid phase separation of patchy particles illuminates diverse effects of regulatory components on protein droplet formation. Scientific reports. 2018; 8(1):1–11. https://doi.org/10.1038/s41598-018-25132-1 PMID: 29712961

72. Chou HY, Aksimentiev A. Single-Protein Collapse Determines Phase Equilibria of a Biological Condensate. The Journal of Physical Chemistry Letters. 2020; 11(12):4923–4929. https://doi.org/10.1021/acs.jpclett.0c01222 PMID: 32426986

73. Ranganathan S, Shakhnovich E. Effect of RNA on morphology and dynamics of membraneless organelles. The Journal of Physical Chemistry B. 2021;. https://doi.org/10.1021/acs.jpcb.1c02286 PMID: 33969989

74. Harmon TS, Holehouse AS, Rosen MK, Pappu RV. Intrinsically disordered linkers determine the interplay between phase separation and gelation in multivalent proteins. elife. 2017; 6:e30294. https://doi.org/10.7554/eLife.30294 PMID: 29091028

75. Das S, Eisen A, Lin YH, Chan HS. A lattice model of charge-pattern-dependent polyampholyte phase separation. The Journal of Physical Chemistry B. 2018; 122(21):5418–5431. https://doi.org/10.1021/acs.jpcb.7b11723 PMID: 29397728

76. Harmon TS, Holehouse AS, Pappu RV. Differential solvation of intrinsically disordered linkers drives the formation of spatially organized droplets in ternary systems of linear multivalent proteins. New Journal of Physics. 2018; 20(4):045002. https://doi.org/10.1088/1367-2630/aab8d9

77. Choi JM, Dar F, Pappu RV. LASSI: A lattice model for simulating phase transitions of multivalent proteins. PLOS Computational Biology. 2019; 15(10):e1007028. https://doi.org/10.1371/journal.pcbi.1007028 PMID: 31634364

78. Lee J, Popov YO, Fredrickson GH. Complex coacervation: A field theoretic simulation study of polyelectrolyte complexation. The Journal of chemical physics. 2008; 128(22):224908. https://doi.org/10.1063/1.2936834 PMID: 18554054

79. Lin YH, Brady JP, Forman-Kay JD, Chan HS. Charge pattern matching as a 'fuzzy'mode of molecular recognition for the functional phase separations of intrinsically disordered proteins. New Journal of Physics. 2017; 19(11):115003. https://doi.org/10.1088/1367-2630/aa9369

80. McCarty J, Delaney KT, Danielsen SP, Fredrickson GH, Shea JE. Complete phase diagram for liquid–liquid phase separation of intrinsically disordered proteins. The journal of physical chemistry letters. 2019; 10(8):1644–1652. https://doi.org/10.1021/acs.jpclett.9b00099 PMID: 30873835

81. Choi JM, Hyman AA, Pappu RV. Generalized models for bond percolation transitions of associative polymers. Physical Review E. 2020; 102(4). https://doi.org/10.1103/PhysRevE.102.042403 PMID: 33212590

82. Weber CA, Zwicker D, Jülicher F, Lee CF. Physics of active emulsions. Reports on Progress in Physics. 2019; 82(6):064601. https://doi.org/10.1088/1361-6633/ab052b PMID: 30731446

83. Blas FJ, MacDowell LG, de Miguel E, Jackson G. Vapor-liquid interfacial properties of fully flexible Lennard-Jones chains. The Journal of chemical physics. 2008; 129(14):144703. https://doi.org/10.1063/1.2989115 PMID: 19045161

84. Silmore KS, Howard MP, Panagiotopoulos AZ. Vapour–liquid phase equilibrium and surface tension of fully flexible Lennard–Jones chains. Molecular Physics. 2017; 115(3):320–327. https://doi.org/10.1080/00268976.2016.1262075

85. Das RK, Pappu RV. Conformations of intrinsically disordered proteins are influenced by linear sequence distributions of oppositely charged residues. Proceedings of the National Academy of Sciences. 2013; 110(33):13392–13397. https://doi.org/10.1073/pnas.1304749110 PMID: 23901099

86. Hazra MK, Levy Y. Charge pattern affects the structure and dynamics of polyampholyte condensates. Physical Chemistry Chemical Physics. 2020; 22(34):19368–19375. https://doi.org/10.1039/D0CP02764B PMID: 32822449

87. Bianchi E, Largo J, Tartaglia P, Zaccarelli E, Sciortino F. Phase diagram of patchy colloids: Towards empty liquids. Physical review letters. 2006; 97(16):168301. https://doi.org/10.1103/PhysRevLett.97.168301 PMID: 17155440

88. Banjade S, Wu Q, Mittal A, Peeples WB, Pappu RV, Rosen MK. Conserved interdomain linker promotes phase separation of the multivalent adaptor protein Nck. Proceedings of the National Academy of Sciences. 2015; 112(47):E6426–E6435. https://doi.org/10.1073/pnas.1508778112 PMID: 26553976

89. Martin EW, Holehouse AS, Peran I, Farag M, Incicco JJ, Bremer A, et al. Valence and patterning of aromatic residues determine the phase behavior of prion-like domains. Science. 2020; 367(6478):694–699. https://doi.org/10.1126/science.aaw8653 PMID: 32029630

90. Ruff KM, Dar F, Pappu RV. Ligand effects on phase separation of multivalent macromolecules. bioRxiv. 2020.

91. Espinosa JR, Garaizar A, Vega C, Frenkel D, Collepardo-Guevara R. Breakdown of the law of rectilinear diameter and related surprises in the liquid-vapor coexistence in systems of patchy particles. J Chem Phys. 2019; 150:224510. https://doi.org/10.1063/1.5098551 PMID: 31202247

92. Russo J, Tavares J, Teixeira P, da Gama MT, Sciortino F. Re-entrant phase behaviour of network fluids: A patchy particle model with temperature-dependent valence. The Journal of chemical physics. 2011; 135(3):034501. https://doi.org/10.1063/1.3605703 PMID: 21787007

93. Farr SE, Woods EJ, Joseph JA, Garaizar A, Collepardo-Guevara R. Nucleosome plasticity is a critical element of chromatin liquid–liquid phase separation and multivalent nucleosome interactions. bioRxiv. 2020.

94. Blas FJ, Galindo A, Vega C. Study of the solid-liquid-vapour phase equilibria of flexible chain molecules using Wertheim's thermodynamic perturbation theory. Molecular Physics. 2003; 101(3):449–458. https://doi.org/10.1080/0026897021000043981

95. Garaizar A, Sanchez-Burgos I, Collepardo-Guevara R, Espinosa JR. Expansion of Intrinsically Disordered Proteins Increases the Range of Stability of Liquid–Liquid Phase Separation. Molecules. 2020; 25(20):4705. https://doi.org/10.3390/molecules25204705 PMID: 33076213

96. Dar F, Pappu R. Phase Separation: Restricting the sizes of condensates. Elife. 2020; 9:e59663. https://doi.org/10.7554/eLife.59663 PMID: 32662769

97. Boeynaems S, Holehouse AS, Weinhardt V, Kovacs D, Van Lindt J, Larabell C, et al. Spontaneous driving forces give rise to protein- RNA condensates with coexisting phases and complex material properties. Proceedings of the National Academy of Sciences. 2019; 116(16):7889–7898. https://doi.org/10.1073/pnas.1821038116 PMID: 30926670

98. Sanchez-Burgos I, Espinosa JR, Joseph JA, Collepardo-Guevara R. Valency and Binding Affinity Variations Can Regulate the Multilayered Organization of Protein Condensates with Many Components. Biomolecules. 2021; 11(2):278. https://doi.org/10.3390/biom11020278 PMID: 33672806

99. Sanchez-Burgos I, Joseph JA, Collepardo-Guevara R, Espinosa JR. Size conservation emerges spontaneously in biomolecular condensates formed by scaffolds and surfactant clients. Scientifc Reports. 2021; 11:15241. https://doi.org/10.1038/s41598-021-94309-y PMID: 34315935

100. Espinosa JR, Joseph JA, Sanchez-Burgos I, Garaizar A, Frenkel D, Collepardo-Guevara R. Liquid network connectivity regulates the stability and composition of biomolecular condensates with many components. Proceedings of the National Academy of Sciences. 2020; 117(24):13238–13247. https://doi.org/10.1073/pnas.1917569117 PMID: 32482873

101. Collepardo-Guevara R, Portella G, Vendruscolo M, Frenkel D, Schlick T, Orozco M. Chromatin Unfolding by Epigenetic Modifications Explained by Dramatic Impairment of Internucleosome Interactions: A Multiscale Computational Study. Journal of the American Chemical Society. 2015; 137 (32):10205–10215. https://doi.org/10.1021/jacs.5b04086 PMID: 26192632

102. Potoyan DA, Papoian GA. Regulation of the H4 tail binding and folding landscapes via Lys-16 acetylation. Proceedings of the National Academy of Sciences. 2012; 109(44):17857–17862. https://doi.org/10.1073/pnas.1201805109 PMID: 22988066

103. Krainer G, Welsh TJ, Joseph JA, Espinosa JR, Wittmann S, de Csilléry E, et al. Reentrant liquid condensate phase of proteins is stabilized by hydrophobic and non-ionic interactions. Nature Communications. 2021; 12(1):1–14. https://doi.org/10.1038/s41467-021-21181-9 PMID: 33597515

104. Su Z, Dhusia K, Wu Y. Coarse-grained simulations of phase separation driven by DNA and its sensor protein cGAS. Archives of Biochemistry and Biophysics. 2021; 710:109001. https://doi.org/10.1016/j.abb.2021.109001 PMID: 34352244

105. Sridhar A, Farr SE, Portella G, Schlick T, Orozco M, Collepardo-Guevara R. Emergence of chromatin hierarchical loops from protein disorder and nucleosome asymmetry. Proceedings of the National Academy of Sciences. 2020; 117(13):7216–7224. https://doi.org/10.1073/pnas.1910044117 PMID: 32165536

106. Sridhar A, Orozco M, Collepardo-Guevara R. Protein disorder-to-order transition enhances the nucleosome-binding affinity of H1. Nucleic acids research. 2020; 48(10):5318–5331. https://doi.org/10.1093/nar/gkaa285 PMID: 32356891

107. Kaur T, Raju M, Alshareedah I, Davis RB, Potoyan DA, Banerjee PR. Sequence-encoded and composition-dependent protein-RNA interactions control multiphasic condensate topologies. bioRxiv. 2020.

108. Alshareedah I, Moosa MM, Raju M, Potoyan DA, Banerjee PR. Phase transition of RNA-protein complexes into ordered hollow condensates. Proceedings of the National Academy of Sciences. 2020; 117(27):15650–15658. https://doi.org/10.1073/pnas.1922365117 PMID: 32571937

109. Kaur T, Raju M, Alshareedah I, Davis RB, Potoyan DA, Banerjee PR. Sequence-encoded and composition-dependent protein-RNA interactions control multiphasic condensate morphologies. Nature communications. 2021; 12(1):1–16. https://doi.org/10.1038/s41467-021-21089-4 PMID: 33558506

110. Damman R, Schütz S, Luo Y, Weingarth M, Sprangers R, Baldus M. Atomic-level insight into mRNA processing bodies by combining solid and solution-state NMR spectroscopy. Nature communications. 2019; 10(1):1–11. https://doi.org/10.1038/s41467-019-12402-3 PMID: 31586050

111. Partridge B, Lee CF. Critical motility-induced phase separation belongs to the Ising universality class. Physical review letters. 2019; 123(6):068002. https://doi.org/10.1103/PhysRevLett.123.068002 PMID: 31491158

112. Garaizar A, Espinosa JR. Salt dependent phase behavior of intrinsically disordered proteins from a coarse-grained model with explicit water and ions. The Journal of Chemical Physics. 2021; 155 (12):125103. https://doi.org/10.1063/5.0062687 PMID: 34598583

113. Wang X, Ramírez-Hinestrosa S, Dobnikar J, Frenkel D. The Lennard-Jones potential: when (not) to use it. Physical Chemistry Chemical Physics. 2020; 22(19):10624–10633. https://doi.org/10.1039/C9CP05445F PMID: 31681941

114. Welsh TJ, Krainer G, Espinosa JR, Joseph JA, Sridhar A, Jahnel M, et al. Single particle zeta-potential measurements reveal the role of electrostatics in protein condensate stability. bioRxiv. 2020.

115. Jover J, Haslam AJ, Galindo A, Jackson G, Müller EA. Pseudo hard-sphere potential for use in continuous molecular-dynamics simulation of spherical and chain molecules. Journal of Chemical Physics. 2012; 137(14). https://doi.org/10.1063/1.4754275 PMID: 23061853

116. Espinosa J, Vega C, Sanz E. The mold integration method for the calculation of the crystal-fluid interfacial free energy from simulations. The Journal of chemical physics. 2014; 141(13):134709. https://doi.org/10.1063/1.4896621 PMID: 25296830

117. Ladd A, Woodcock L. Triple-point coexistence properties of the Lennard-Jones system. Chemical Physics Letters. 1977; 51(1):155–159. https://doi.org/10.1016/0009-2614(77)85375-X

118. García Fernández R, Abascal JLF, Vega C. The melting point of ice Ih for common water models calculated from direct coexistence of the solid-liquid interface. The Journal of Chemical Physics. 2006; 124(14):144506. https://doi.org/10.1063/1.2183308 PMID: 16626213

119. Rowlinson JS, Widom B. Molecular theory of capillarity. Courier Corporation; 2013.

120. Espinosa JR, Joseph JA, Garaizar A, Sanchez-Burgos I, Frenkel D, Collepardo-Guevara R. Liquid-network connectivity regulates the stability and composition of biomolecular condensates with many components.

121. Bond CS, Fox AH. Paraspeckles: nuclear bodies built on long noncoding RNA. Journal of Cell Biology. 2009; 186(5):637–644. https://doi.org/10.1083/jcb.200906113 PMID: 19720872

122. Gomes E, Shorter J. The molecular language of membraneless organelles. Journal of Biological Chemistry. 2019; 294(18):7115–7127. https://doi.org/10.1074/jbc.TM118.001192 PMID: 30045872

123. Wang A, Conicella AE, Schmidt HB, Martin EW, Rhoads SN, Reeb AN, et al. A single N-terminal phosphomimic disrupts TDP-43 polymerization, phase separation, and RNA splicing. The EMBO journal. 2018; 37(5):e97452. https://doi.org/10.15252/embj.201797452 PMID: 29438978

124. Niaki AG, Sarkar J, Cai X, Rhine K, Vidaurre V, Guy B, et al. Loss of dynamic RNA interaction and aberrant phase separation induced by two distinct types of ALS/FTD-linked FUS mutations. Molecular cell. 2020; 77(1):82–94. https://doi.org/10.1016/j.molcel.2019.09.022 PMID: 31630970

125. Kim Y, Myong S. RNA remodeling activity of DEAD box proteins tuned by protein concentration, RNA length, and ATP. Molecular cell. 2016; 63(5):865–876. https://doi.org/10.1016/j.molcel.2016.07.010 PMID: 27546789

126. Fisher RS, Elbaum-Garfinkle S. Tunable multiphase dynamics of arginine and lysine liquid condensates. Nature communications. 2020; 11(1):1–10. https://doi.org/10.1038/s41467-020-18224-y PMID: 32934220

127. Saha S, Weber CA, Nousch M, Adame-Arana O, Hoege C, Hein MY, et al. Polar positioning of phase-separated liquid compartments in cells regulated by an mRNA competition mechanism. Cell. 2016; 166(6):1572–1584. https://doi.org/10.1016/j.cell.2016.08.006 PMID: 27594427

128. Khong A, Matheny T, Jain S, Mitchell SF, Wheeler JR, Parker R. The stress granule transcriptome reveals principles of mRNA accumulation in stress granules. Molecular cell. 2017; 68(4):808–820. https://doi.org/10.1016/j.molcel.2017.10.015 PMID: 29129640

129. Namkoong S, Ho A, Woo YM, Kwak H, Lee JH. Systematic characterization of stress-induced RNA granulation. Molecular cell. 2018; 70(1):175–187. https://doi.org/10.1016/j.molcel.2018.02.025 PMID: 29576526

130. Fox AH, Nakagawa S, Hirose T, Bond CS. Paraspeckles: where long noncoding RNA meets phase separation. Trends in biochemical sciences. 2018; 43(2):124–135. https://doi.org/10.1016/j.tibs.2017.12.001 PMID: 29289458

131. Clemson CM, Hutchinson JN, Sara SA, Ensminger AW, Fox AH, Chess A, et al. An architectural role for a nuclear noncoding RNA: NEAT1 RNA is essential for the structure of paraspeckles. Molecular cell. 2009; 33(6):717–726. https://doi.org/10.1016/j.molcel.2009.01.026 PMID: 19217333

132. Ancona M, Brackley CA. Simulating the chromatin mediated phase separation of model proteins with multiple domains. arXiv preprint arXiv:210714518. 2021.

133. Wang Y, Zhou H, Sun X, Huang Q, Li S, Liu Z, et al. Charge segregation in the intrinsically disordered region governs VRN1 and DNA liquid-like phase separation robustness. Journal of Molecular Biology. 2021; p. 167269. https://doi.org/10.1016/j.jmb.2021.167269 PMID: 34571015

134. Alshareedah I, Thurston GM, Banerjee PR. Quantifying viscosity and surface tension of multicomponent protein-nucleic acid condensates. Biophysical Journal. 2021;. https://doi.org/10.1016/j.bpj.2021.01.005 PMID: 33453268

135. Yu M, Lemke EA. There is plenty of room in protein-RNA condensates. Biophysical Journal. 2021;. https://doi.org/10.1016/j.bpj.2021.02.024 PMID: 33691085

136. Zhang H, Elbaum-Garfinkle S, Langdon EM, Taylor N, Occhipinti P, Bridges AA, et al. RNA controls PolyQ protein phase transitions. Molecular cell. 2015; 60(2):220–230. https://doi.org/10.1016/j.molcel.2015.09.017 PMID: 26474065